



HAL
open science

Microstructural design of new high conductivity – high strength Cu-based alloy

Stéphane Gorsse, Blanche Ouvrard, Mohamed Gouné, Angeline Poulon-Quintin

► **To cite this version:**

Stéphane Gorsse, Blanche Ouvrard, Mohamed Gouné, Angeline Poulon-Quintin. Microstructural design of new high conductivity – high strength Cu-based alloy. *Journal of Alloys and Compounds*, 2015, 633, pp.42-47. 10.1016/j.jallcom.2015.01.234 . hal-01122713

HAL Id: hal-01122713

<https://hal.science/hal-01122713>

Submitted on 9 Jan 2019

HAL is a multi-disciplinary open access archive for the deposit and dissemination of scientific research documents, whether they are published or not. The documents may come from teaching and research institutions in France or abroad, or from public or private research centers.

L'archive ouverte pluridisciplinaire **HAL**, est destinée au dépôt et à la diffusion de documents scientifiques de niveau recherche, publiés ou non, émanant des établissements d'enseignement et de recherche français ou étrangers, des laboratoires publics ou privés.



Distributed under a Creative Commons Attribution - NonCommercial - NoDerivatives 4.0 International License

Microstructural design of new high conductivity – high strength Cu-based alloy

S. Gorsse*, B. Ouvrard, M. Gouné, A. Poulon-Quintin

CNRS, Université de Bordeaux, ICMCB,

87 avenue du Docteur Albert Schweitzer, 33608 Pessac Cedex, France

Abstract:

Some novel high conductivity-high strength materials were designed in the binary Cu-Mg. They exhibit an excellent balance between strength and electrical properties. The properties and the performance of the designed materials are compared with the main Cu-based alloys and the analysis shows that they perform equally to the best one (Cu-Be). Furthermore, we show that an increase of Mg content modifies the microstructure feature and leads to a strong increase of strength without any significant deterioration of the electrical conductivity. This behavior was attributed to the formation of eutectic islands in which high density of Cu₂Mg nanoparticles precipitate.

1. Introduction

Copper-based high strength conductive alloys are used in a myriad of applications in automotive, aeronautic and electronic industries such as conductive springs, interconnections, etc [1]. The demand of these materials is booming, partly driven by the increase use of copper in existing applications but also by energy and environmental considerations where their uses in emerging applications such as electrical propulsion and renewable energy are essential. The strongest conductive alloy is based on the Cu-Be system

[2] which has the disadvantage of toxicity and cost. There is a great demand for the replacement of Cu-Be alloys by new toxic free and environmentally friendly high strength-high conductivity materials.

Among the different approaches proposed to develop high strength and increase electrical conductivity of Cu alloys, severe plastic deformation leading to ultrafine grained microstructure and nanoscale precipitation of a secondary phase are the most investigated for solute having a very limited solubility in Cu such as Cu-Cr [3,4,5] and Cu-Ag [6], for example. In an attempt to find an alternative, we focused on the Cu-Mg system for two main reasons (1) Mg affects only weakly the electrical conductivity of Cu [7] and (2) in contrast with Cu-Cr and Cu-Ag, it provides several degree of freedom to generate microstructures (eutectic transformation, driving forces for precipitation). Studies of Cu-Mg alloys are not numerous and mainly limited to the aging response of low alloyed compositions [8, 9, 10, 11] apart from the work of Fehrenbach et al. [12] and Fidler et al. [13] on the eutectic transformation.

In order to obtain high strength – high conductivity materials, an alloy design was performed in the Cu-Mg system from the thermodynamic properties of the studied system. Then, different compositions of Mg (4.1at%, 8.1at%, 23.1at%) were selected and the evolution of microstructural, electrical and mechanical properties were investigated. It was shown that the obtained materials exhibit an excellent balance between strength and electrical conductivity properties and an increase of Mg contents leads to a strong increase of strength without any significant deterioration of the conductivity. The origin of such properties is discussed from a metallurgical point of view.

2. Selection of the studied compositions in the Cu-Mg binary system

There are several experimental and thermodynamic descriptions of the Cu-Mg system in the literature [14,15,16]. The most recent results agree that the Cu-Mg system consists of the liquid, the terminal solid solutions: fcc (Cu solid solution), hcp (Mg solid solution), and the intermetallic compounds Cu_2Mg and CuMg_2 (**Fig.1**). Both intermetallic phases melt congruently and are involved in eutectic reactions with either fcc or hcp solid solutions. We have used the thermodynamic parameters evaluated from the CALPHAD assessment of Coughanowr et al. [14] in which Cu_2Mg is described by the sublattice model $(\text{Cu,Mg})_2(\text{Cu,Mg})$ and the compound energy formalism in order to reproduce the homogeneity range, whereas CuMg_2 is considered as a line compound.

Adding any solute to Cu leads to a decrease of its electrical conductivity because the local perturbation of both the atomic and electronic structure of the perfect crystal around the impurity atoms acts as scattering centers for electrons. The scattering effect increases with the difference of size and valence between the solute and the host atoms, this is why the residual resistivity arising from impurities increases as the position of the solute element becomes distant from that of a host component in a given line of the periodic table [17]. More precisely, the residual resistivity is a function of the scattering cross section of the impurity which increases as the square of the valency difference between the impurity and the host metal [18]. In the case of Mg, the excess valency is only of 1 which is enough to disrupt the uniform charge of Cu and screens the conduction electron. The magnitude of the screening radius is given by $(6\pi e^2 \rho_0 / E_F)^{-1/2}$, where E_F is the Fermi energy and ρ_0 the density of conduction electrons [19]. With the values of $E_F = 7\text{eV}$ and $\rho_0 = 8.5 \cdot 10^{28}/\text{m}^3$ for pure Cu, this gives a magnitude of the screening radius of about 0.055 nm which is much shorter than the interatomic distance of 0.255 of pure Cu and leads to an increase of the resistivity. According to Nordheim's rule [20] the residual resistivity is proportional to the impurity concentration.

However, the presence of the Cu_2Mg compound provides a mean to decrease the amount of the residual solute since an important fraction of Mg will leave the Cu lattice to form the corresponding secondary phase. Secondary phase particles scatter electrons too with an effect that depends on their size and spacing (compared to the electron mean free path), though not as much as solute atoms.

In order to evaluate the effect of the microstructure (solute atoms, secondary phase, grain boundaries) on properties, three alloy compositions were selected to cover the main features of the Cu-Mg phase diagram (see **Figure 1**):

- (1) Cu-4.1at%Mg, on cooling this alloy will not cross the eutectic line leading to the formation of a single-phase fcc-Cu solid solution of composition identical to that of the alloy,
- (2) Cu-8.1at%Mg, on cooling the liquid phase will reach the eutectic composition and the alloy will end in the two-phase field fcc-Cu + Cu_2Mg ,
- (3) Cu-23.1at%Mg that is close to the eutectic composition.

3. Experimental procedure

The Cu-Mg alloys were prepared by induction melting of Cu (99.99%) and Mg (99.9%) pieces in a glassy carbon crucible under argon. This way, small ingots with 16 mm in diameter and 30 mm in height were obtained. Metallographic examination was performed by scanning electron microscopy (SEM) on a polished sample. Phase identification was made using X-ray diffraction (XRD) and electron probe microanalysis (EPMA).

The electrical conductivity was determined at room temperature by the linear four probe method and the hardness by Vickers micro-indentation [21]. A load of 1.96 N was applied with

a rate of 40 $\mu\text{m/s}$ and maintained during 20 seconds. Each measurement was taken 10 times. This hardness have been converted to yield strength from the Taylor Factor [22].

4. Experimental results and discussion

Figure 2 presents the SEM backscattered electron (BSE) images of the Cu-4.1at%Mg, Cu-8.1at%Mg and Cu-23.1at%Mg alloy compositions in the as-cast condition. The phase with the lowest mean atomic number (Mg content) appears darkest in the image. The sample Cu-8.1at%Mg consists of Cu-rich dendrites surrounded by a lamellar structure of alternating Cu-rich (bright) and Mg-rich (dark) phases. The interlamellar spacing is about 0.8 μm and the size of the dendrites is about 23 μm . EPMA indicates that the mean composition of the dendrites is 4.3 at.% Mg, the bright lamella is 7.7 at.% Mg, and the dark lamella is 31.5 at.% Mg. The analysis of the XRD spectra shown in the **Figure 3** indicates that the microstructure is composed by a solid solution of fcc-Cu(Mg) and the intermetallic compound Cu_2Mg .

The samples Cu-4.1at%Mg consists of the single-phase fcc-Cu(Mg) solid solution having the nominal composition of the alloy. The microstructure of the Cu-23.1at%Mg is composed of a fully lamellar aggregates of alternating fcc-Cu(Mg) with composition 7.7at% Mg and Cu_2Mg phases with a constant lamellar spacing of about 1 μm . The measured compositions of the lamellae in the eutectic aggregates are reported in the **Figure 1** (see black circle).

Both these latter and the formation of a lamellar pattern typical of an eutectic transformation confirm the phase fields, the invariant reaction and the solubility limits of the calculated Cu-Mg phase diagram in the Cu-rich side.

Two different morphologies can be distinguished for second phase (here Cu_2Mg) particles at grain boundaries of matrix (here Cu). Indeed, the lens-like shape would be favored if the grain

boundary energy of grains in the matrix per unit area is smaller (two times at least) than the energy per unit of the Cu/Cu₂Mg interphase boundary. Otherwise, a layer of Cu₂Mg phase wets continuously the Cu/Cu grain boundary for the reason that the growing Cu₂Mg phase particle tends to increase its surface. Even if the grain boundary wetting has already been observed in phase transformations such as both the eutectoid and eutectic transformations [23,24], in our study, we did not observe any particular wetting of Cu₂Mg at any grain boundary (see **Figure 2**). This situation is radically different from that one observed in a fully eutectic microstructure in the Zn-Al system [24]. A close examination of the **Figure 2** shows the complete coverage of primary Cu₂Mg grain by copper. However, this is a minor and does not accurately reflect the final microstructure feature. Furthermore, it is worth noting that the morphology of the Cu₂Mg shall be mainly determined by the morphology of Cu that is mainly lenticular with a large range of aspect ratio. In other words, the resulting microstructure feature is very similar to that one of pearlite in steels in which lamella of Fe₃C is embedded in α -Fe matrix.

The proportion of the eutectic aggregates evaluated from image analysis of the Cu-8.1at%Mg alloy is 25 vol.% that is 28 mol.%, which is above the 8 mol.% calculated under equilibrium condition (lever rule). This difference may arise from a kinetics effect. Indeed, the composition of the solid as a function of the fraction of the solid is given by the Scheil-Gulliver equation : $C_s = kC_0(1 - f_s)^{k-1}$, where C_s is the composition of the solid, C_0 is the nominal composition, k is the partition coefficient ($k = C_s/C_l$, with C_l the liquid composition) and f_s is the fraction of the solid.

Figure 4 shows the calculated composition changes as a function of the fraction of solid: as the amount of solid increases during solidification, the Mg concentration of the liquid increases until it reaches the eutectic composition C_E to form a lamellar structure. Therefore,

The fraction of the eutectic aggregates can be obtained when the composition of the liquid is equal to the eutectic composition (0.21 at fraction). The **Figure 4** shows that this situation happens when the fraction of the eutectic phase is about 30 mol.%. This latter is in very good agreement with the experimentally determined one (28 mol.%).

The analysis performed by Electron Probe MicroAnalyser given in **Figure 5** evidences a gradient of Mg composition around the eutectic islands. The Mg content being much higher close to the interface between eutectic islands and Cu than in the bulk (6.9 at% vs 3.1at %).

Since the amount of Mg in the alloy is above the maximum solubility of Mg in Cu, it can be reasonably supposed that precipitation of a second phase occurs during cooling. In order to check this assumption, some analysis by TEM were performed on the Cu-23.1at%Mg alloy.

The results given in **Figure 6** evidence the presence of nanoparticles in Cu. The TEM images show a high density of particles having a very small mean size (around 5nm to 15nm). The comparison between the obtained Selected Area Electron Diffraction pattern (**Figure 7**) of a zone located in copper lamellar and some simulated diffraction pattern of Cu_2Mg along various zone axis, would indicate that precipitates correspond to Cu_2Mg . This high density of particles observed in our samples can be explained by the enhancement of the driving force for Cu_2Mg nucleation close to the interface resulting to a higher Mg content as observed in **Figure 5**.

Figure 8 shows the bubble chart (Ashby's diagram) of yield strength and electrical conductivity for the alloys prepared in this study in comparison with the main Cu-based alloys. It is observed that the addition of Mg to Cu leads to a decrease of its electrical conductivity and an increase of its yield strength. The importance of this effect depends on the amount of Mg and then on the resulting microstructure. One can see that the present Cu-Mg alloys occupy the same field than Cu-Be alloys which suggest that they perform equally well with respect to this

combination of properties. It is also noticeable that the Cu-23.1at%Mg alloy exhibit an exceptionally high yield strength combined with a good electrical conductivity.

The decrease of the electrical conductivity of copper with the addition of Mg is due to the scattering of electrons. Mg solute atoms act as scattering centers, when their number increases the electron mean free path decreases. The effect is very significant between pure copper and the Cu-4.1at%Mg alloy since all the Mg added goes into solid solution. For compositions above the solubility limit, the additional amount of Mg is removed from the liquid to form the Cu_2Mg compound. This explains why there is only a slight decrease of the electrical conductivity from 4.1 to 23.1 at% Mg.

In order to explain this high value of the yield strength, we have adapted a mechanical model initially developed to describe the mechanical behavior of perlite, an eutectoid microstructure composed by lamella of Fe_3C [25]. Indeed, a parallel can be drawn between the microstructure of the present copper alloy in which grains of fcc-Cu(Mg) and lamellar eutectic aggregates replace the ferrite and the pearlite in low carbon steels. From this model it is possible to account the hardening contribution that arise from:

- the solid solution, it depends on the amount of Mg solute into the copper grains,
- the grain boundaries, this is the so-called Hall-Petch hardening being inversely proportional to the square root of the grain size,
- the eutectic aggregates leading to hardening by composite effect, it is related to the interlamellar spacing and the volume fraction of the eutectic structure.

For the Cu-4.1at%Mg alloy, which consists of a single-phase solid solution with grain size of 23 μm , the evolution of the flow stress σ_{Cu} as a function of the strain ε_{Cu} is expressed as follows [25]:

$$\sigma_{Cu}(\varepsilon_{Cu}) = \sigma_0^{Cu} + \frac{\alpha\mu M\sqrt{b}}{\sqrt{d}} \sqrt{\frac{1 - \exp(-fM\varepsilon_{Cu})}{f}}$$

with α a constant equals to 0.4, M the Taylor factor ($M = 3$), μ the shear modulus of copper ($\mu = 46$ GPa), b the Burger's vector ($b = 0.255$ nm) and d the mean copper grain size ($d = 23$ μ m). f is an adjustable parameter taken from [25]. σ_0^{Cu} is the summation of the intrinsic lattice resistance, a value of 40 MPa is used (pure copper) [2], and the solid solution strengthening effect that arises from the addition of Mg atoms in the Cu lattice. This effect is proportional to the amount of solute and can be evaluated as CX_{ss} , where X_{ss} is the mole fraction of Mg in solid solution and $C = 49$ MPa/X to reproduce the measured value of the yield strength for the Cu-4.1at%Mg (**Fig. 9**). We can conclude from this result that the contribution arising from Mg solute atoms is the dominant hardening mode in the single phase Cu-4.1at%Mg alloys.

The increase of the amount of Mg solutes leads to the formation of lamellar aggregates in the Cu-8.1at%Mg alloy due to the eutectic transformation. The law to describe the strengthening effect of the lamellar pattern is expressed as follows [25]:

$$\sigma_{eut}(\varepsilon_{eut}) = \sigma_0^{eut} + \frac{\mu Mb}{S} + \frac{K}{g} \left(1 - \exp\left(-\frac{g\varepsilon_{eut}}{2}\right)\right)$$

Where K and g are two empirical constants taken from Ref.19, and S is the interlamellar spacing ($S = 0.8$ μ m), and σ_0^{eut} is the critical stress due to the lattice friction in the copper lamellae of the eutectic aggregates. From the measured Mg concentration in the copper lamella and the value of C (proportionality coefficient for the solid solution strengthening effect) determined from the analysis of the Cu-4.1at%Mg alloy, the numerical value of σ_0^{eut} is 418 MPa.

As shown in **Figure 9**, the summation of the different strengthening contributions arising from the intrinsic lattice resistance, the solid solution, the grain boundaries, and the eutectic

aggregates leads to a value of about 330 MPa which is below the measured yield strength (459 MPa) for the Cu-8.1at%Mg alloy. The same trend is observed for the Cu-23.1at%Mg alloy which consists of 100% of eutectic aggregates. The gap between the calculated and measured values, 524 and 1024 MPa respectively, is even higher, and can be attributed to the distribution of precipitates as seen in the TEM dark field image in **Figure 6**. Indeed, it is well known that particles can have an attractive interaction with dislocation and act to pin the dislocation, giving rise to a strengthening effect. In order to evaluate the possible contribution to the strengthening provided by precipitates, one can calculate the mean particle spacing in the slip plane, λ , leading to a stress increment τ of 500 MPa by considering the bowing of dislocations between precipitates:

$$\lambda \approx 0.8M \frac{\mu b}{\tau_{Orowan}}$$

where M is the Taylor Factor (M=3), μ is the shear modulus of copper ($\mu=48$ GPa) and b is the Burgers vector (b=0.25 nm). The determined mean particle spacing λ is about of 50nm. This value, qualitatively consistent with our TEM observations (**Figure 6**), requires a high density of nanoparticles in Cu matrix.

5. Conclusion

Some novel high conductivity – high strength materials were designed in the binary Cu-Mg. They exhibit an excellent balance between strength and electrical properties. An increase of Mg content leads to a strong increase of strength (more than 1000MPa) without any

significant deterioration of the electrical conductivity. This unexpected behavior is attributed to the formation of eutectic islands $\text{Cu}_2\text{Mg}/\text{Cu}$ in which high density of Cu_2Mg nanoparticles precipitate during cooling. The design material is a good alternative to the Cu-Be system which has the disadvantage of toxicity.

The microstructure designed in the binary Cu-Mg exhibits both a high conductivity and high strength. These properties were obtained from a classical process. The High Pressure Torsion technic would opens up new opportunities. Indeed, as nicely shown by [26] it could be thus possible to control the precipitation state including the size of particle and the composition of the matrix by acting on the rotation angle. The latter control the properties of both strengthening and electrical properties.

Acknowledgements

The research was supported by The French National Research Agency (ANR-08-JCJC-0133).

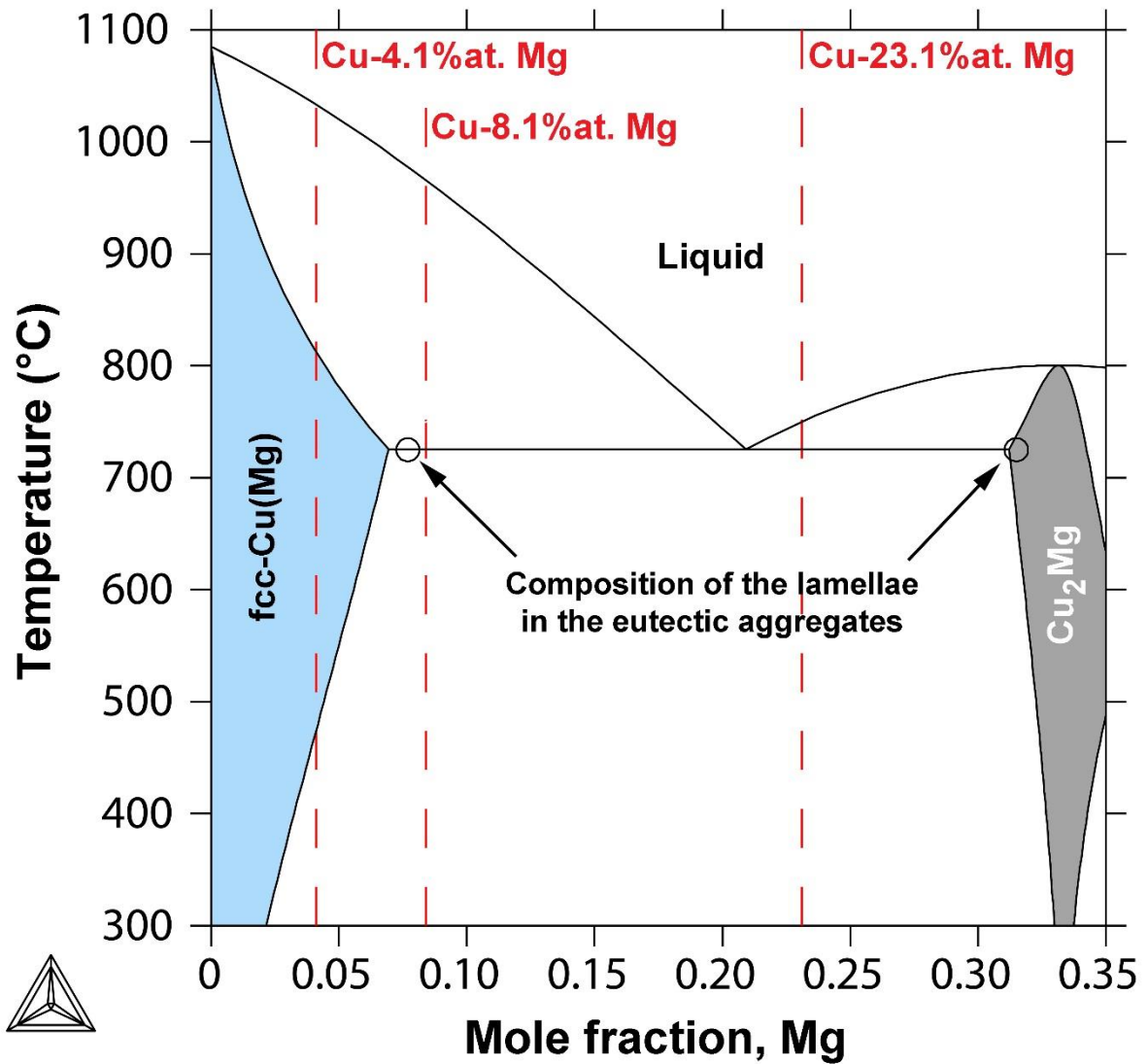
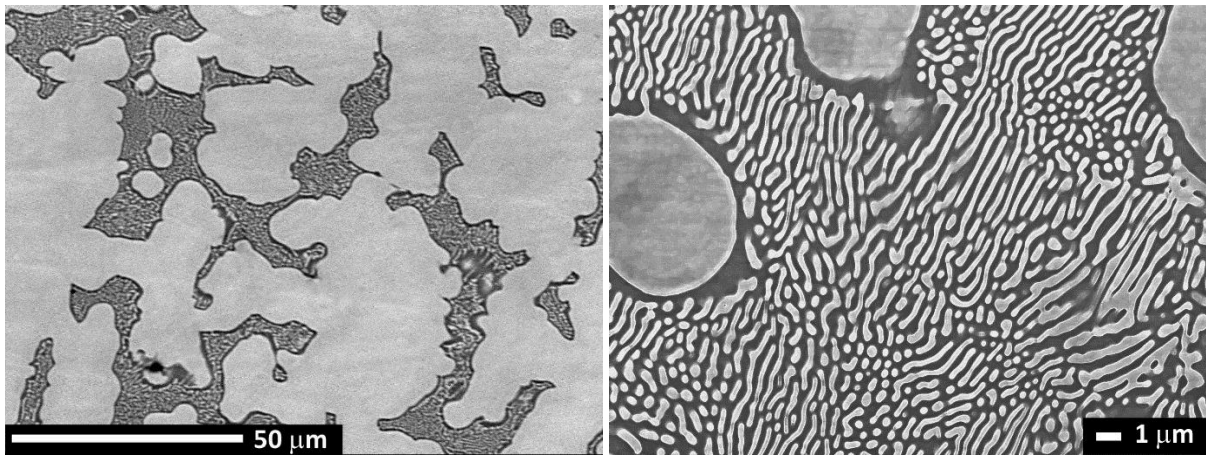
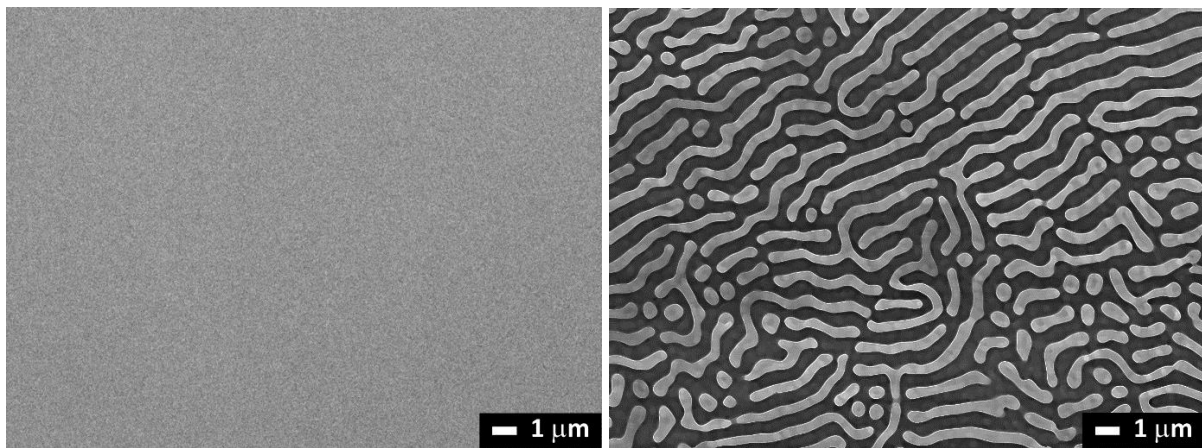


Figure 1: Binary phase diagram of the Cu-Mg system calculated using ThermoCalc and the thermodynamic evaluation of Coughanowr et al. [14]. The open circles indicate the measured composition of the lamellae in the eutectic aggregates.



(a)

(b)



(c)

(d)

Figure 2: SEM micrographs of (a) the as-cast Cu-8.1at%Mg alloy, (b) a zoom of the eutectic aggregates, (c) the Cu-4.1at%Mg alloy, and (d) the Cu-23.1at% alloy. The α -Cu(Mg) solid solution and Cu_2Mg appear in light and dark gray, respectively.

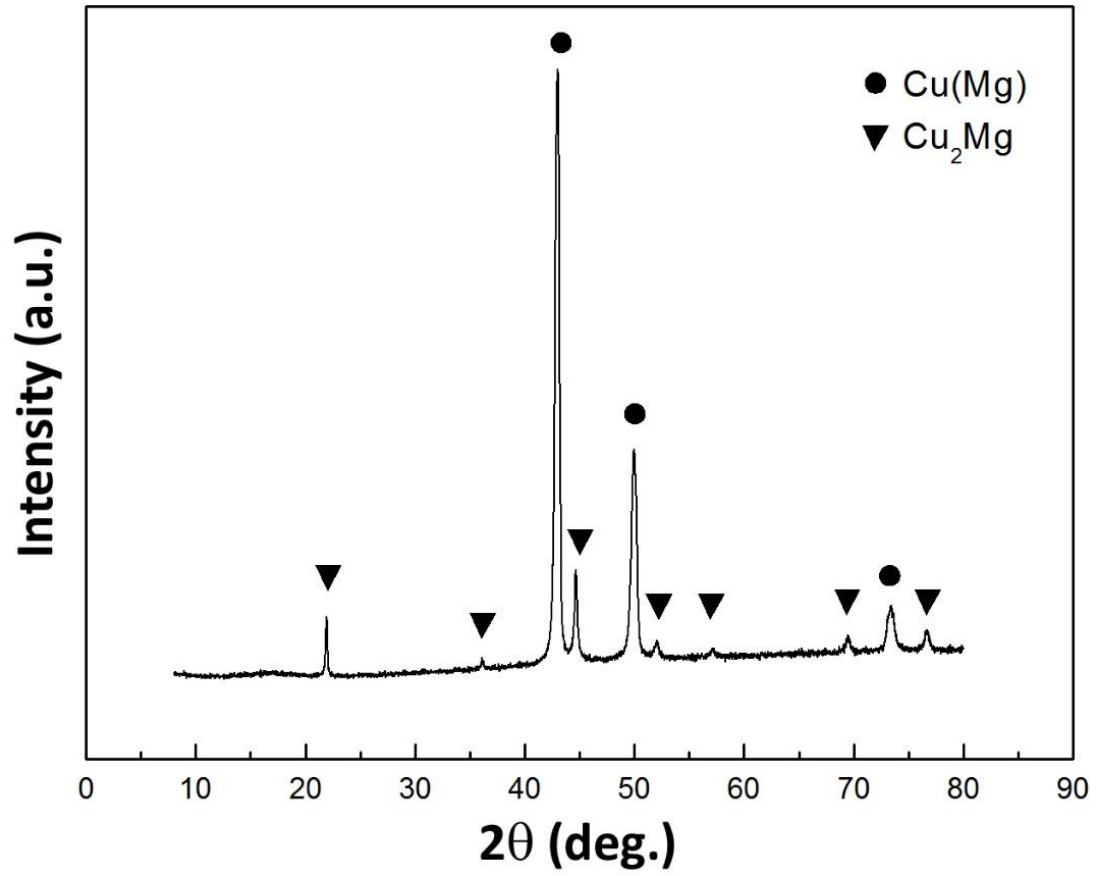


Figure 3: XRD spectra corresponding to the microstructural state shown in Fig.2a for the as-cast Cu-8.1at%Mg alloy.

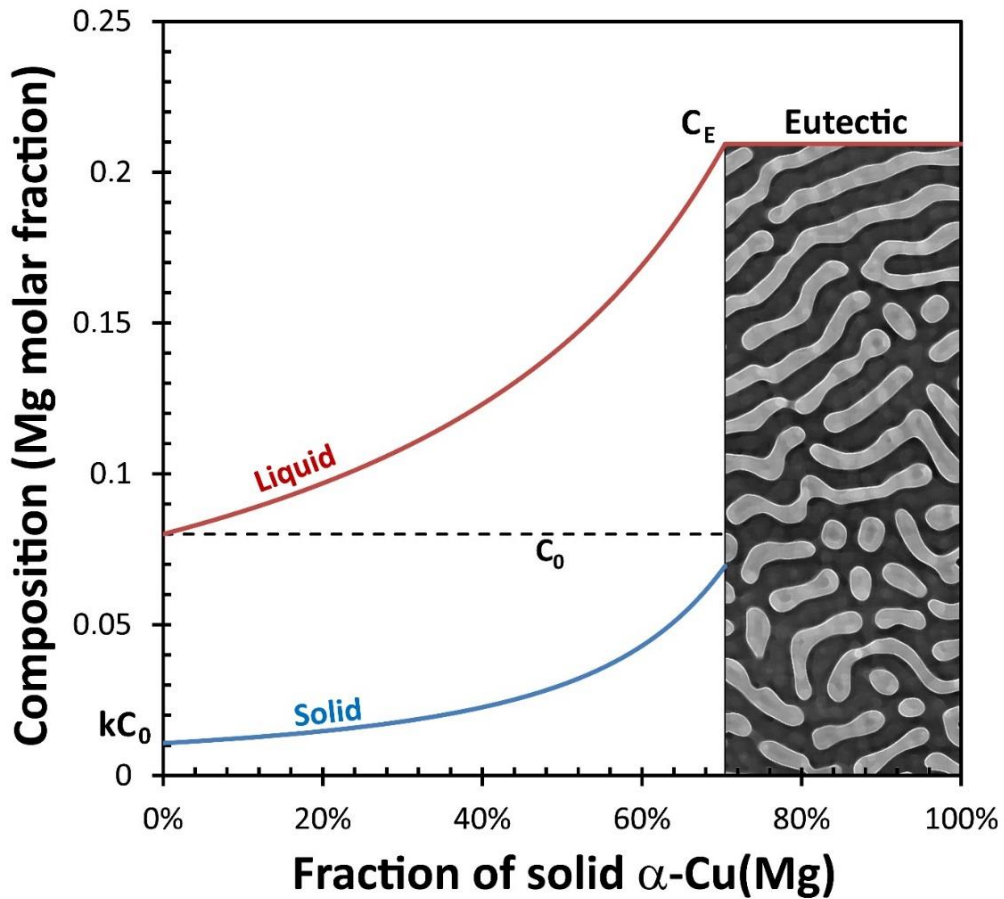


Figure 4: Solute profile according the Scheil-Gulliver equation. When the solid begins to form, the solute (Mg) is rejected into the liquid phase ahead of the solid/liquid interface. Since it is redistributed into the liquid only by diffusion, there is an accumulation of this solute in the liquid until the eutectic composition C_E is reached, leading to the formation of a lamellar mixture of α -Cu(Mg) (light gray) and Cu_2Mg (dark gray).

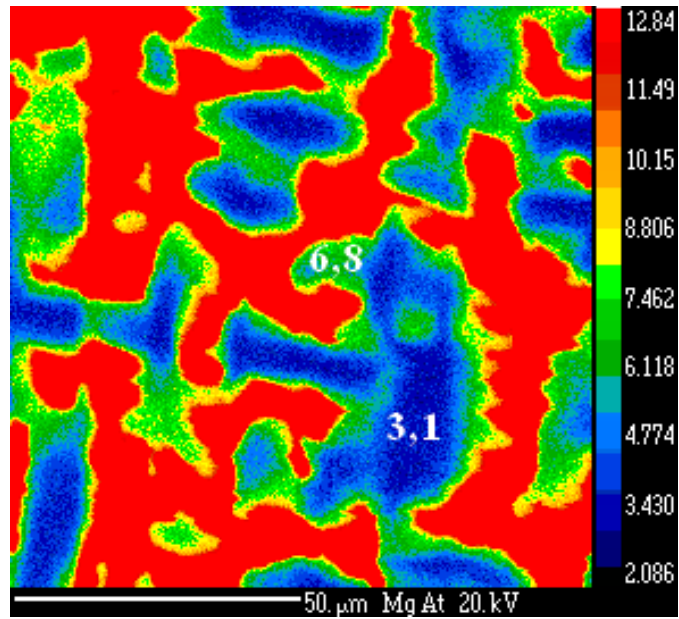


Figure 5: Analysis of the Mg content in the Cu-8.1 at%Mg by Electron Probe Micro Analyser. The Mg content is heterogeneous in Copper. It is much more higher close to the interface between the eutectic islands (6.3 at%) than in the bulk (3. 1at%).

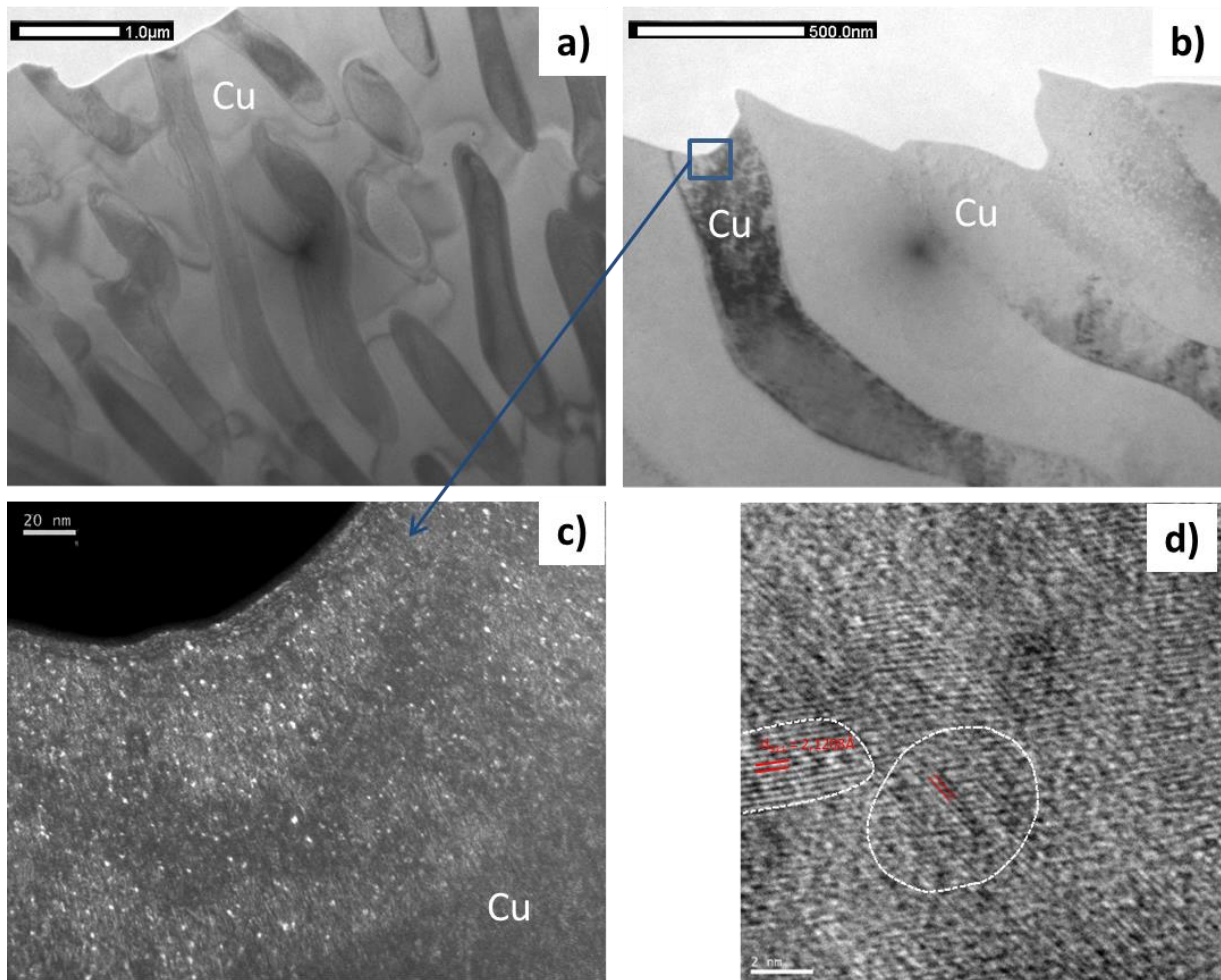


Figure 6: a) TEM images of the fully eutectic microstructure (Cu-23.1at%Mg), b) Bright field and associated c) dark field inside the copper matrix. Both the dark field (c) and the HRTEM image (d) show the presence of high density of nanoparticles in copper identified as Cu_2Mg .

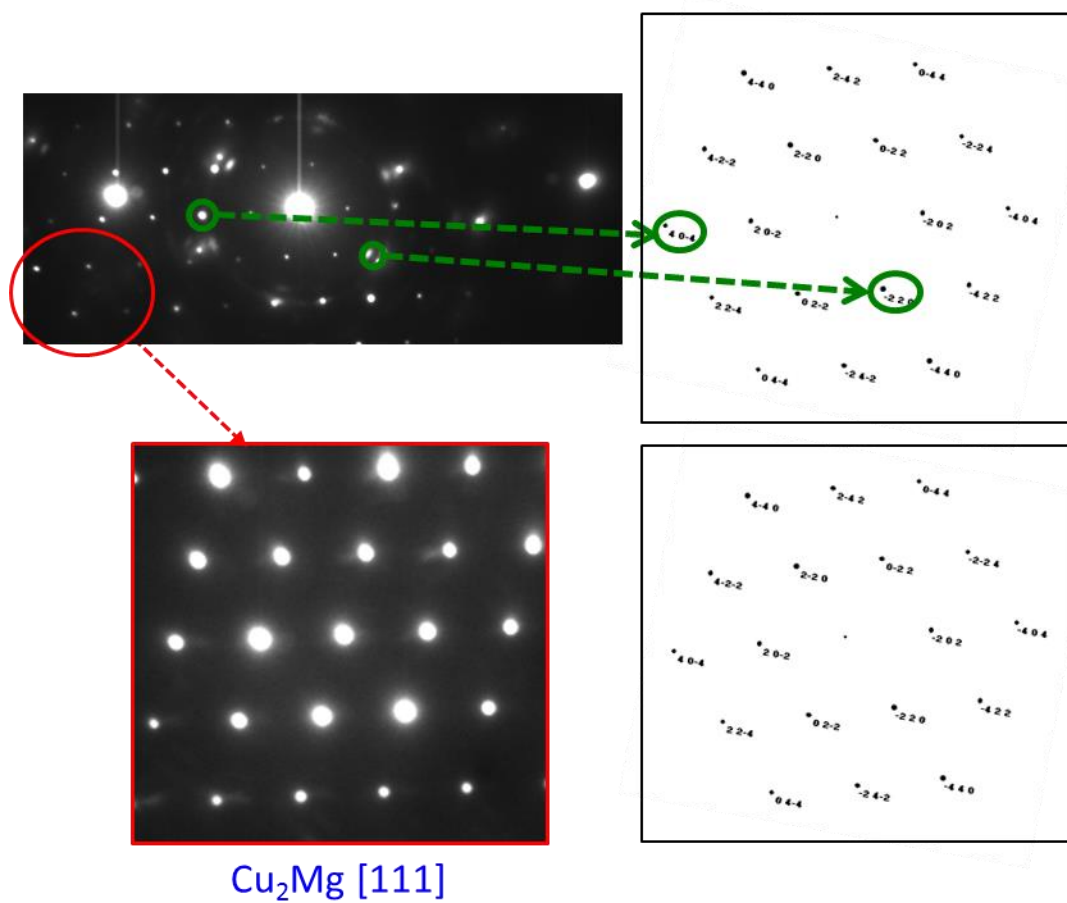


Figure 7: Comparison between the obtained Selected Area Electron Diffraction and the microdiffraction pattern of Cu_2Mg along different zone axis. These results would indicate that precipitates corresponds to Cu_2Mg .

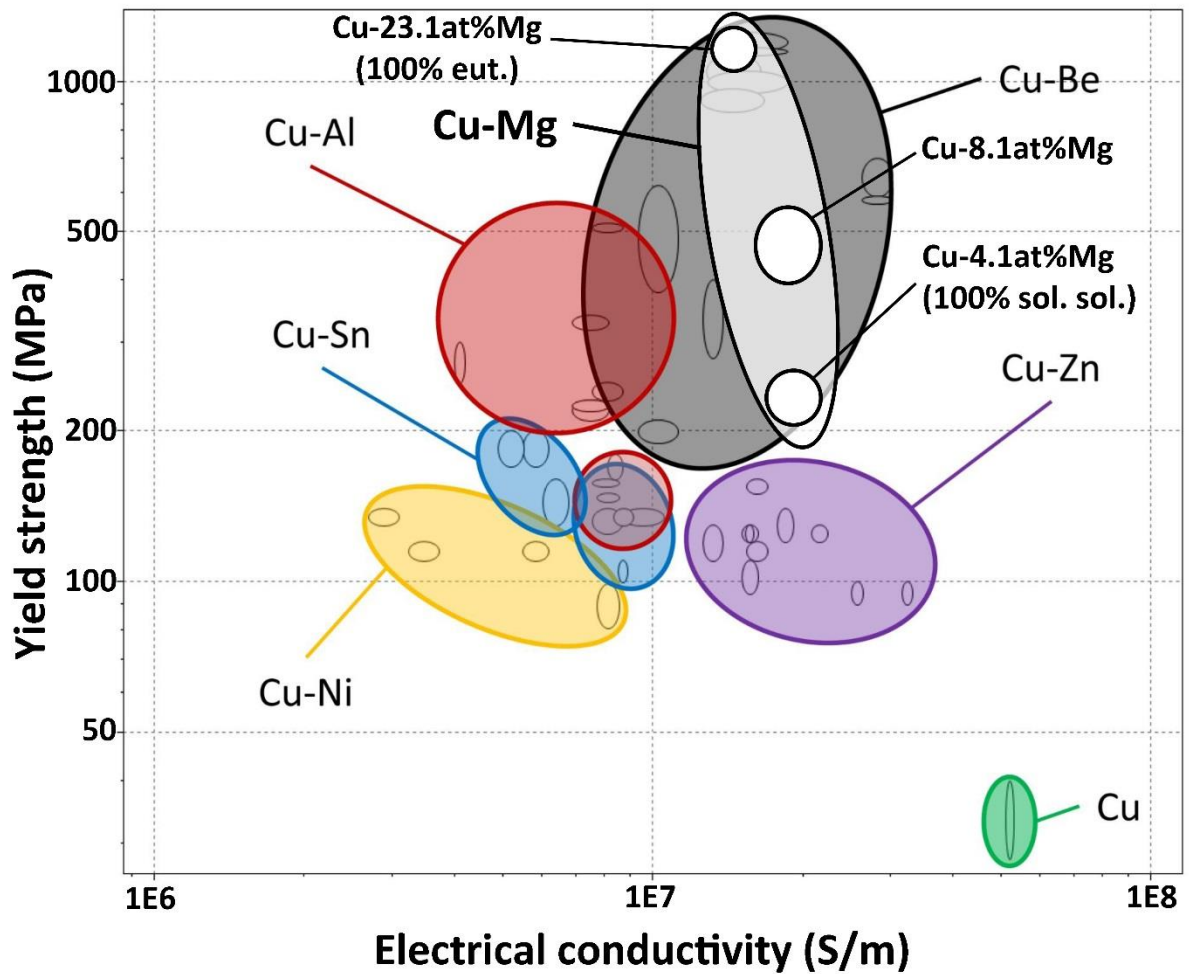


Figure 8: Logarithmic plot of the yield strength vs. electrical conductivity for copper based alloys according [2] and the casted Cu-4.1at%Mg, Cu-8.1at%Mg and Cu-23.1at%Mg alloys from the present work. The best choices for high strength and high conductivity are Cu-Be alloys and the present alloys.

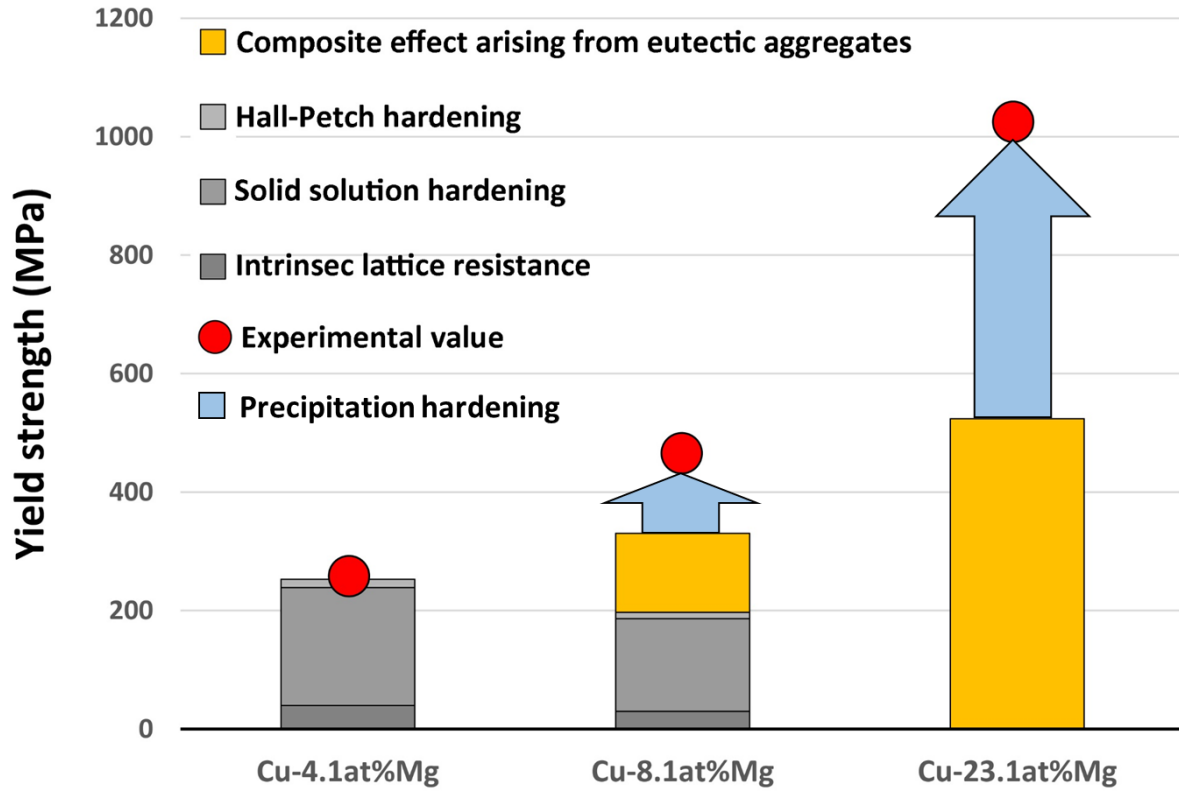


Figure 9: Calculated strengthening contributions for the casted Cu-Mg alloys: Cu-4.1at%Mg is a single-phase fcc-Cu(Mg) solid solution, Cu-8.1at%Mg is composed of fcc-Cu(Mg) and eutectic aggregates, and Cu-23.1at%Mg consists of fully eutectic structure.

References

- 1 - Copper Applications Technology Roadmap, International Copper Association, March 2011.
- 2 - CES Edupack 2013 database (software), Granta Design Ltd, Cambridge, UK.
- 3 - N. Takata, Y. Ohtake, K. Kita, K. Kitagawab and N. Tsuji, *Scripta Mater.* 60 (2009) 590.
- 4 - R. K. Islamgaliev,^{1,a} K. M. Nesterov,¹ J. Bourgon,² Y. Champion,² and R. Z. Valiev, *J. Appl. Phys.* 115 (2014) 194301.
- 5 - A. Chbihi, X. Sauvage, D. Blavette, *Acta Mater.* 60 (2012) 4575.
- 6 - K. S. Raju, V. S. Sarma, A. Kauffmann, Z. Hegeduse, J. Gubicza, M. Peterlechner, J. Freudenberger, G. Wilde, *Acta Mater.* 61 (2013) 228.
- 7 - Y. Zeng, S. Mu, P. Wu, K.P. Ong, and J. Zhang, *J. Alloys Compd.*, 478 (2009) 345.
- 8 - O. Dahl, *Siemens-Konzern* 6 (1927) 222.
- 9 - H. Böhm, *Z. Metallkd.* 52 (1961) 564.
- 10 - H. Tsubakino and R. Nozato, *J. Mater. Sci.* 19 (1984) 3013.
- 11 - K.-I. Nishikawa, S. Semboshi, and T. J. Konno, *Solid State Phenomena* 127 (2007) 103.
- 12 - PJ Fehrenbach, HW Kerr, and P Niessen, *J. Cryst. Growth*, 18 (1973) 151.
- 13 - R.S Fidler, M.N Croker, and R.W Smith, *J. Cryst. Growth*, 13-14 (1972) 739.
- 14 - C. Coughanowr, I. Ansara, R. Luoma, M. Hämmäläinen, H.L. Lukas, *Z. Metallkd.* 82 (1991) 574.
- 15 - T. Buhler, S.G. Fries, and P.J. Spencer, *J. Phase Equilibria* 19 (1998) 317.
- 16 - S. Gorsse and G.J. Shiflet, *Calphad* 26 (2002) 63.
- 17 - A.L. Norbury, *Trans. Faraday Soc.* 16 (1921) 570.
- 18 - G.T. Meaden, *Electrical resistance of metals*, Plenum Press, New York, 1965 (Chapter 5).

-
- 19 - F. Seitz, *The Modern Theory of Solids* (McGraw-Hill, New York, 1940).
- 20 - J.S. Galsin, Kluwer/Plenum Publishers, New York, 2002, 109.
- 21 - P. Dordor, E. Marquestaut, C. Salducci, P. Hagenmuller, *Rev. Phys. Appl.* 20 (1985) 795.
- 22 - Y. Champion and Y. Bréchet, *Adv. Eng. Mater.* 12 (2010) 798.
- 23 - J.W. Christian, *The theory of transformations in metals and alloys*, Oxford: Pergamon Press, 1975, 452.
- 24 - G.A. Lopez, E. J. Mittemeijer, B.B. Straumal, *Acta Mater.* 52 (2004) 4537.
- 25 - S. Allain and O. Bouaziz, *Mater. Sci. Eng. A* 496 (2008) 329.
- 26 - B.B. Straumal, A. R. Kilmametov, Y. Ivanisenko, L. Kurmanaeva, B. Baretzky, Y. O. Kucheev, P. Zieba, A. Korneva, D. A. Molodov, *Materials Letters* 118 (2014) 111.